



Improved PV module model for dynamic and nonuniform climatic conditions in ISIS-proteus

Alaeddine Ahmed Azi¹ · Djamel Saigaa² · Mahmoud Drif² · Abdelouadoud Loukriz³ · Ahmed Bendib⁴ · Moadh Kichene⁵

Received: 8 June 2024 / Accepted: 25 July 2024

© The Author(s), under exclusive licence to Springer-Verlag GmbH Germany, part of Springer Nature 2024

Abstract

Modeling and simulating photovoltaic (PV) cells or modules involve using mathematical and computational models to predict their behavior and performance under various conditions. This can include modeling the electrical characteristics of solar cells, as well as the interactions between multiple cells in a PV module. In ISIS-Proteus software, the existing research works have modeled the PV modules either by using a Proteus Spice model of the PV panel without including the effect of climatic conditions variation or by using pure mathematical relations that describe all physical and environmental parameters that lead to a static behavior. Therefore, this paper proposes a new improved ISIS-Proteus model of a PV cell/module for dynamic performance emulation under varying climatic conditions. The proposed model is designed based on the equivalent circuit of a five-parameter single-diode as an electrical part controlled by a numerical part that includes the mathematical expressions corresponding to each parameter. The designed model can capture the impact of solar irradiance and temperature on PV outputs, thereby enhancing real-world PV performance prediction. Also, it can effectively simulate the effect of the partial shading. To validate the accuracy of the proposed model, a comparative study is conducted evaluating the model's performance against PVsyst software models and real-world data brought from a large-scale grid-connected PV station in Ain El-Melh, Algeria. In this study, the simulation tests are carried out using ISIS-Proteus considering several PV module types and under various operating conditions, including uniform test conditions (UTCs) and partial shading conditions (PSCs). The findings, including I–V and P–V curves and several standard metrics, prove the proposed model's effectiveness in accurately predicting the behavior of PV modules under both UTCs and PSCs, aligning closely with real-world performance.

Keywords ISIS-Proteus software · I–V curve · Modeling · Partial shading condition (PSC) · PV module · P–V curve

List of symbols

✉ Abdelouadoud Loukriz
abdelouadoud.loukriz@usthb.edu.dz
Alaeddine Ahmed Azi
alaeddine.ahmedazi@univ-biskra.dz
Djamel Saigaa
Djamel.saigaa@univ-msila.dz
Mahmoud Drif
Mahmoud.drif@univ-msila.dz
Ahmed Bendib
ahmeddib28@gmail.com
Moadh Kichene
kichenemoadh@usto.dz

¹ Laboratoire de Modélisation des Systèmes Energétiques (LMSE), Mohamed KHIDER University, BP 7000, Biskra, Algeria

A Modified ideality factor
 A_{ref} Modified ideality factor at STC
 E_g Material band-gap energy (eV)
 $E_{g,ref}$ Material band-gap energy at STC (eV)
 n Diode ideality factor
 G Solar irradiance (W/m²)

² University Mohamed Boudiaf of M'sila, BP166, 28000 M'sila, Algeria

³ University of Science and Technology Houari Boumediene, Bab Ezzouar, BP No. 32 El Alia, Bab Ezzouar, 16111 Algiers, Algeria

⁴ University of Blida, Blida, Algeria

⁵ Department of Electrical Engineering, USTO-MB University, Oran, Algeria

G_{ref}	Solar irradiance at STC (= 1000W/m ²)
I	Cell current (A)
I_d	Diode current (A)
$I_{\text{ph,ref}}$	Photocurrent of the solar cell at STC (A)
I_0	Reverse saturation current of the solar cell at operation conditions (A)
$I_{0,\text{ref}}$	Reverse saturation current of the solar cell at STC (A)
I_{sc}	Short-circuit current of the solar cell at operation conditions (A)
$I_{\text{sc,ref}}$	Short-circuit current of the solar cell at STC (A)
I_p	Parallel resistance current (A)
k	Boltzmann's constant (1.38×10^{-23} J/K)
q	Electron charge (1.602×10^{-19} C)
R_s	Series resistance of the PV cell (Ω)
$R_{s,\text{ref}}$	Series resistance of the PV cell at STC (Ω)
$R_{s,m}$	Series resistance of the PV module (Ω)
$R_{s,m,\text{ref}}$	Series resistance of the PV module at STC (Ω)
R_p	Parallel resistance of the PV cell (Ω)
$R_{p,\text{ref}}$	Parallel resistance of the PV cell at STC (Ω)
$R_{p,m}$	Parallel resistance of the PV module (Ω)
$R_{p,m,\text{ref}}$	Parallel resistance of the PV module at STC (Ω)
T	Cell temperature at operation conditions ($^{\circ}\text{C}$)
T_{ref}	Cell temperature at operation conditions at STC (= 25 $^{\circ}\text{C}$)
V	Cell voltage (V)
V_d	Diode voltage (V)
k_i	Temperature coefficient of the short-circuit current (mA/ $^{\circ}\text{C}$)
k_v	Temperature coefficient of the open-circuit voltage (mV/ $^{\circ}\text{C}$)
k_p	Temperature coefficient of the power (%/ $^{\circ}\text{C}$)
<i>STCs</i>	Standard test conditions (AM1.5, 1000W/m ² , 25 $^{\circ}\text{C}$)
<i>UTCs</i>	Uniform test conditions
<i>LMPP</i>	Local maximum power point
<i>GMPP</i>	Global maximum power point

1 Introduction

Solar energy is a crucial renewable energy source (RES) which differs from nonrenewable sources like gasoline and coal in being clean, inexhaustible, and free. Photovoltaic (PV) systems are primarily used either as stand-alone systems for applications such as water pumping, domestic and street lighting, electric vehicles, military and space applications, or as grid-connected systems like hybrid systems and power plants [1, 2]. Through a physical mechanism known as the photoelectric effect, a PV cell directly transforms solar

energy into electrical energy [3, 4]. Additionally, the current–voltage (I–V) characteristics of the PV cell resemble the exponential behavior of a PN junction, indicating the presence of an interface between the N-type and P-type semiconductor material types inside the semiconductor [4]. Since the open-circuit voltage of the PV cell depends on the semiconductor gap and not on the size, there will always be a 0.6 V across an open-circuited cell [5]. Therefore, many cells have to be connected in series to form a PV panel which can then be associated to form a larger unit called an array. However, the PV panel or cell circuit model must be studied to analyze its electrical behavior [6, 7].

In the existing literature, several researchers have addressed the PV panel circuit modeling including the single-diode and double-diode equivalent circuit models [9]. Anani et al. [10] have employed numerical techniques to calculate the lumped-circuit parameters of a single-diode model under standard test conditions (STC). They utilized MATLAB/Simulink to evaluate the method's performance across various weather conditions. In addition, Bouraiou et al. [11] have presented models of single- and double-diode configurations using MATLAB/Simulink, and have validated their model's accuracy through experimental data spanning different irradiance and temperature values. Ciulla et al. [12] discussed five PV panel models including single, double, and three-diode configurations, employing an algorithm to extract PV model parameters and analyze their relationship with the electrical behavior under varying weather conditions. Franzitta et al. [13] and Hovinen [14] have used hypotheses, mathematical equations, and operational procedures to extract single-diode circuit parameters using analytical techniques. Laudani et al. [15] have proposed a rapid and accurate method to extract single-diode circuit parameters based on datasheet information and experimental I–V curves, simplifying the complexity associated with mathematical considerations in parameter extraction for PV cells or panels. However, the single-diode model is often favored for its simplicity and effectiveness in representing the equivalent circuit of PV panels or cells. This model has been extensively discussed and analyzed by Muhammadsharif et al. [7], highlighting its balance between accuracy and computational efficiency. On the other hand, to fully characterize a PV panel, it is essential to accurately obtain and analyze its current–voltage (I–V) and power–voltage (P–V) curves under varying environmental conditions using appropriate software tools [16]. For this, Chatterjee et al. [17] have demonstrated the use of MATLAB m-file to generate and analyze the I–V and P–V curves of a single-diode PV cell across different irradiance and temperature levels. Further, advancements have been made by Ma et al. [18] by developing a simulation model for PV power generation systems. Their simulations, conducted under various environmental conditions, have been validated against outdoor test results,

illustrating the I–V characteristics of the model. Moreover, Ma et al. [19] have proposed a novel theoretical model aimed at creating a simple and accurate PV model. This model, implemented in MATLAB, has been used to determine the PV module's parameters, with validation against experimental I–V curves under different irradiance and temperature conditions.

From the software point of view, MATLAB/Simulink is often used to model the mathematical equations governing PV circuits, facilitating the analysis of their characteristics and the generation of I–V and P–V curves for diverse atmospheric conditions. For instance, Ding et al. [20] have integrated an S-Function builder within MATLAB/Simulink to illustrate the I–V and P–V characteristics of PV panels under varying environmental conditions, enhancing the tool's capability to simulate and analyze PV system performance. In addition, Yaqoob et al. [21] have introduced a novel approach for modeling single- and double-diode configurations across a range of solar irradiance levels and temperatures. Their method utilizes MATLAB/Simulink's "Multiplexer and Functions blocks," integrated within the MATLAB library. Furthermore, Nguyen and al. [22] have proposed a systematic algorithm for modeling and simulating PV cells, panels, and arrays, offering a detailed step-by-step approach. Basha et al. [23] have employed MATLAB/Simulink to simulate both single- and double-diode models, examining the output power and current characteristics of PV cells under varying solar irradiance and temperature conditions. Their findings highlight that the double-diode model achieves superior efficiency compared to the single-diode model. On the other hand, numerous researchers have explored different methods to characterize PV cell behavior by using the PSIM simulation tool. Chao et al. [24] have developed a PV panel model within the PSIM software package, configuring a PV system of 3 kW rated power to analyze I–V and P–V characteristics under both normal and abnormal weather conditions. Salman et al. [25] have employed a physical model simulator embedded in PSIM to model and simulate a PV panel, resulting in a straightforward yet precise model. They extracted I–V and P–V curves for various environmental conditions and compared simulation outcomes with laboratory test results. In [26], El Hammoumi et al. used PSIM to mathematically model and simulate a PV system, focusing on obtaining PV panel characteristics. They validated their simulations using real-time instrumentation with Arduino data acquisition. However, simulation tools like PSIM and MATLAB/Simulink often lack electronic boards or microcontrollers such as Arduino, FPGA, and DSP, which are essential for testing and implementing practical PV system applications like sun-tracking systems and maximum power point tracking (MPPT) algorithms. This discrepancy between software capabilities and real-world system requirements may lead to operational issues

[27], as the responsiveness of real system components may differ from those of simulated ones. This mismatch may result in increased debugging time for runtime errors. However, such challenges can be effectively addressed using electronic circuit design software tools like Proteus, which provides a platform for integrating microcontrollers into simulations. This enables more accurate emulation of real-world PV system applications such as sun-tracking systems and MPPT algorithms, facilitating thorough testing and validation before practical implementation.

Proteus offers comprehensive capabilities including PCB design, schematic capture, and PROSPICE simulation models. It supports algorithm development on embedded boards like Arduino, FPGA, and PIC directly from its library, allowing for easy programming and simulation mirroring real-world scenarios. Proteus is favored for its extensive electronic component library, providing accurate simulations that closely reflect practical implementations. Compared to tools like MATLAB/Simulink or PSIM, Proteus eliminates the need for algorithm rewriting during practical implementation, making it ideal for thorough system analysis and evaluation before deployment. Despite these benefits, the Proteus software tool lacks a built-in PV panel or cell model in its library, prompting several researchers to develop their models within the software. Among them, Yan et al. [28] have introduced a PV panel model in Proteus to illustrate I–V and P–V curves, focusing on studying partial shading effects. This model uses components like voltage-controlled current sources, diodes, shunt resistors, and series resistors. However, it did not account for the impact of weather conditions on solar PV panel operation. In response, Chalh et al. [29] have presented a new PV panel model using a single-diode equivalent circuit in Proteus. This model incorporates a controlled current source and a diode with customized Spice code to simulate PV panel behavior. However, parameters such as saturation current, number of cells, ideality constant, and band-gap energy have been fixed at a constant temperature of 25 °C, limiting its applicability under varying temperature conditions. Similarly, Yaqoob et al. [30] developed a two-diode equivalent circuit PV panel model in Proteus, but faced challenges with temperature variability during simulation, resulting in limitations under different temperature conditions. In [31], Motahhir et al. developed an innovative PV panel model using Proteus software, incorporating a flexible approach that allows for varying weather conditions based on the mathematical equations of a single-diode equivalent circuit. However, a significant limitation of this model is its inability to account for the effects of partial shading on the performance of the solar PV panel.

Despite the merits of prior research efforts, many studies have approached the modeling of PV modules within a limited scope. Some have employed a Proteus Spice model of the PV panel but overlooked the influence of climatic variations,

especially the partial shading effects. To bridge this gap, a new PV model tailored for dynamic performance simulation within ISIS-Proteus software is developed in this paper. Distinguishing itself from static models, the proposed approach dynamically simulates PV behavior amidst fluctuating climatic conditions using the single-diode equivalent circuit. The main contributions made in this paper are:

- Development of a new PV model for dynamic performance emulation within the ISIS-Proteus software. In contrast to static models, the proposed model allows dynamical simulation of PV behavior considering fluctuating climatic conditions based on the single-diode equivalent circuit (SDM). By incorporating the influence of solar irradiance and temperature variations, the model offers improved real-world performance prediction for PV systems.
- The model's ability to accurately account for the PS effect, which is crucial in real-world PV installations, is investigated. The study shows minimal disparities between the proposed model and PV_{sys} or real data characteristics when subjected to varying shading levels, highlighting the model's efficacy in capturing the complex dynamics of PS of a PV module or string.

The remainder of the paper is organized as follows. An overview of PV system modeling and the PS effect are discussed in Sect. 2, highlighting the nonlinearity of the PV I–V and P–V characteristics. Section 3 describes the proposed model including electrical and numerical parts. Section 4 presents the application and simulation outcomes of the newly proposed model through the ISIS-Proteus software. Section 5 gives the paper's conclusion.

2 Overview of PV system modeling and PS effect

2.1 PV cell

Solar cells are basically P–N junctions fabricated in thin wafers or semiconductor layers. Exposure a cell to sunlight, photons with energy greater than the band-gap energy are absorbed by the semiconductor and generate several electron–hole pairs proportional to the incident solar irradiance. Under the influence of the electric field inside the P–N junction, these charge carriers are swept away and generate a photocurrent proportional to solar irradiance. Besides, PV systems inherently exhibit nonlinear I–V and P–V characteristics that vary with radiation and cell temperature [29].

The equivalent electrical circuit representing the single-diode model of a PV cell in the direct mode under a positive voltage is shown in Fig. 1. This model consists of a cur-

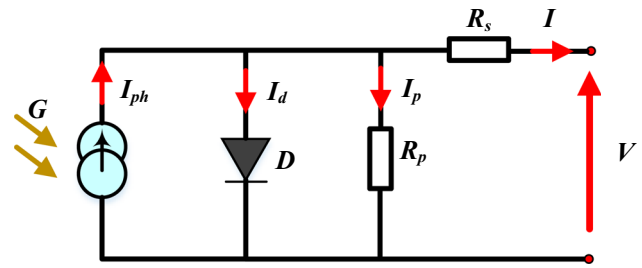


Fig. 1 Equivalent single-diode model of a PV Cell

rent source proportional to the solar irradiance intensity, a paralleled diode that models the P–N junction, a parallel resistance, R_p , expressing a leakage current, and a series resistance, R_s , describing an internal resistance to the current flow. From this figure, the voltage–current characteristic of a solar cell can be mathematically described as follows:

$$I = I_{ph} - I_0 \left(e^{\left(\frac{V + R_s I}{A} \right)} - 1 \right) - \frac{V + R_s I}{R_p} \quad (1)$$

where I and V are the PV output current and voltage, and I_p is the parallel resistance current. I_{ph} is the photocurrent that mainly depends on the solar irradiance (G) and the cell's working temperature (T), I_0 is the reverse cell saturation current that depends also on the cell's working temperature, I_d is the diode current, and A is an ideal factor. These later parameters and the resistances R_s and R_p can be expressed as follows [16]:

$$I_{ph} = [I_{sc} + k_i(T - T_{ref})] \times \frac{G}{G_{ref}} \quad (2)$$

$$I_0 = I_{0-ref} \times \left(\frac{T}{T_{ref}} \right)^3 e^{\left[\left(\frac{qE_g}{nk} \right) \left(\frac{1}{T_{ref}} - \frac{1}{T} \right) \right]} \quad (3)$$

$$I_d = I_0 \left(e^{\left(\frac{V + R_s I}{A} \right)} - 1 \right) \quad (4)$$

$$A = \frac{T}{T_{ref}} A_{ref} \quad (5)$$

$$R_p = \frac{G_{ref}}{G} R_{p-ref} \quad (6)$$

$$R_s = R_{s-ref} \quad (7)$$

where G_{ref} , T_{ref} , I_{0-ref} , and R_{p-ref} are the values of parameters at STC, I_{sc} is the short-circuit current, n is the diode ideality factor, and E_g is the gap energy under STC. q is an electron charge equal to 1.6×10^{-19} C, k is a Boltzmann's constant with the value 1.38×10^{-23} J/K, and A_{ref} is the ideal factor at STC given by :

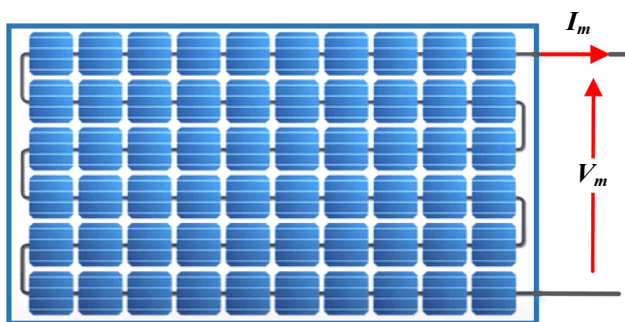


Fig. 2 A typical module of 60 cells connected in series

$$A_{ref} = \frac{nkT_{ref}}{q} \tag{8}$$

2.2 PV module

A PV module consists of multiple individual solar cells connected, often in series, to increase the power and voltage above that of a single solar cell as Fig. 2 illustrates. The number of solar cells connected in series within a module can vary depending on the manufacturer and desired output voltage. Note that an individual silicon solar cell has a voltage at the MPP of around 0.5 V under 25 °C and AM1.5 illuminations.

Considering (1), the expression relates the PV module’s output voltage, V_m , to its current, I_m , can be derived as:

$$I_m = I_{ph-m} - I_0 \left(e^{\left(\frac{V_m + R_{s-m} I_m}{A_m} \right)} - 1 \right) - \frac{V_m + R_{s-m} I_m}{R_{p-m}} \tag{9}$$

where the module’s parameters are defined as follows:

$$\begin{aligned} I_{ph-m} &= I_{ph}; & A_m &= N_s A; & R_{s-m} &= N_s R_s; \\ & & & & R_{p-m} &= N_s R_p \end{aligned}$$

2.3 PV Module under PSCs

The PS shading often occurs when only a portion of a PV module or array receives sunlight while other parts are shaded, significantly affecting system performance and efficiency. Under such a condition, shaded cells within a PV module or array generate less electrical current compared to unshaded cells, leading to reduced overall PV output power. PS commonly arises from various factors such as obstructions like trees or buildings casting shadows on PV modules, passing clouds intermittently blocking sunlight, uneven soiling on modules, or module damage. These factors result

in nonuniform illumination across the array, causing varying levels of electrical current generation. Understanding the impact of PS on PV arrays is essential for optimizing system design and operation to minimize its effects and maximize energy production. Strategies like using bypass diodes, optimizing array orientation, and employing advanced shading analysis tools can help mitigate PS effects and enhance overall system performance.

To clarify the effect of the PS, a string consisting of three PV modules connected in series, presented in Fig. 3a, is analyzed considering V–I and P–V responses. In this figure, each PV module is equipped with bypass diodes in parallel to prevent hot spots, while the series-connected blocking diode is used to avoid other strings operating as load [32]–33. In addition, as seen these PV modules operate under varying solar irradiance levels of 1000, 700, and 300 W/m². The resulting I–V curves for each module are presented in Fig. 3b, while the string I–V and P–V characteristics are illustrated in Fig. 3c. This figure demonstrates that the inclusion of bypass diodes leads to the appearance of multiple MPPs under PSCs.

3 Proposed model of PV module in ISIS-proteus

As mentioned in the introductory section, all existing models of a PV module implemented in ISIS-Proteus software do not take into account the effect of the PS and have considered only PV operating under UTCs. Therefore, a novel general and accurate model of a PV module is proposed to precisely mimic the behavior of the PV module under PSCs. Figure 4 displays the schematic diagram of the implemented system in ISIS-Proteus including the proposed model, which is designed to simulate the electrical characteristics of a PV module. In this scheme, the proposed model considers as inputs various manufacturer-provided parameters under STCs, which are summarized in Table 1, and outputs the current and voltage vectors to print the I–V and P–V curves.

The block diagram of the proposed model in ISIS-Proteus is shown in Fig. 5, which is composed of two parts; electrical and numerical. The electrical part, depicted in Fig. 6, is represented by a five-parameter one-diode equivalent circuit, which is the equivalent circuit of a PV cell of Fig. 1, while the numerical part, given in Fig. 7, includes the mathematical Eqs. (2)–(6), which are in charge of generating the control signals of the electrical part.

It is worth mentioning that in the electrical part, the photo- and diode currents, I_{ph} and I_d , are modeled using a linear voltage-controlled current source (VCCS) with a gain set to 1, while (5) and (6) are implemented using a linear voltage-controlled resistance (VCR) to modify R_s and R_p .

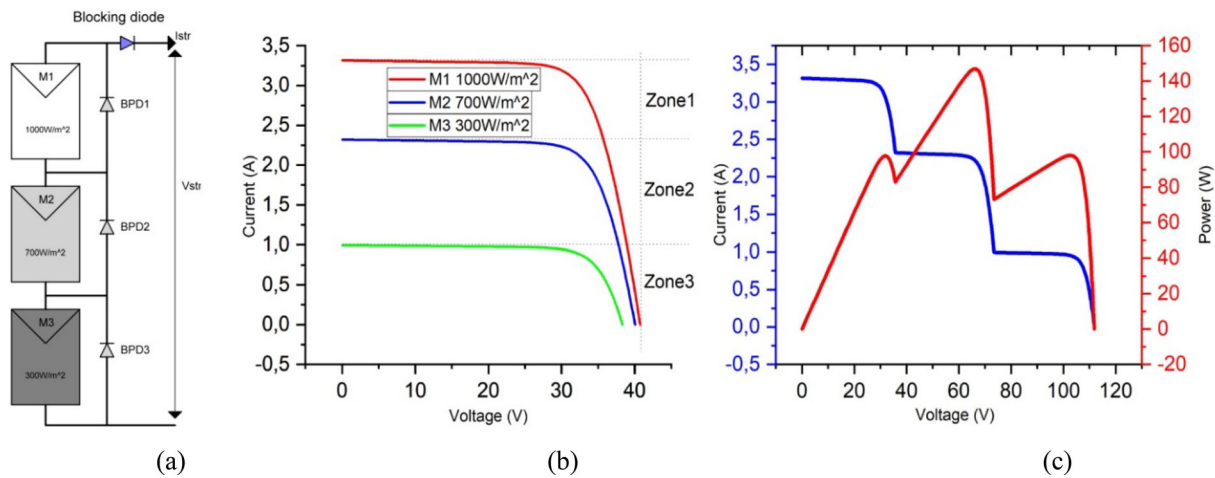


Fig. 3 String of 3 × 1 module operating under three different radiation levels, a partial shaded String, b PV modules I–V curve, and c string I–V, P–V curves

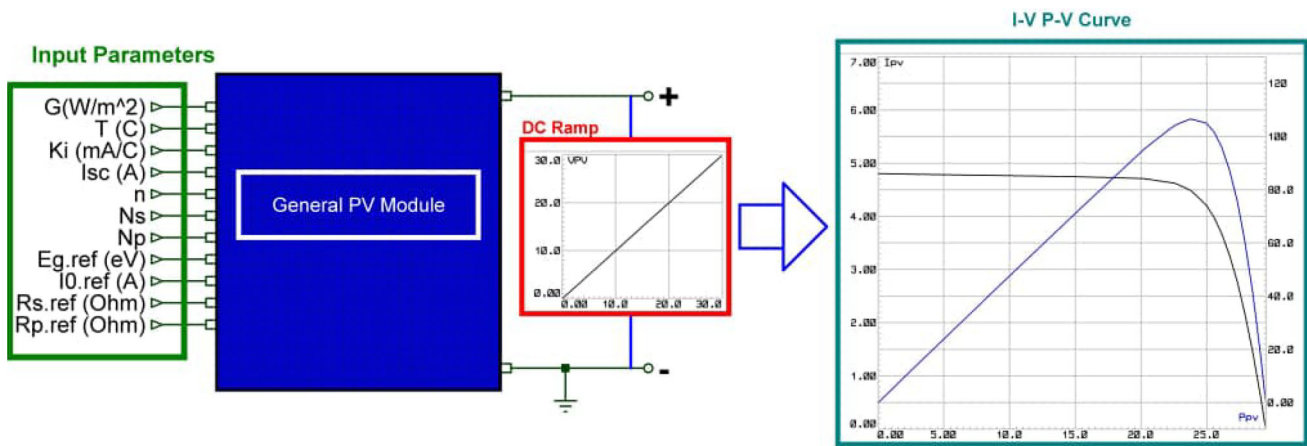


Fig. 4 Implementation of d PV module modeling under ISIS-Proteus software

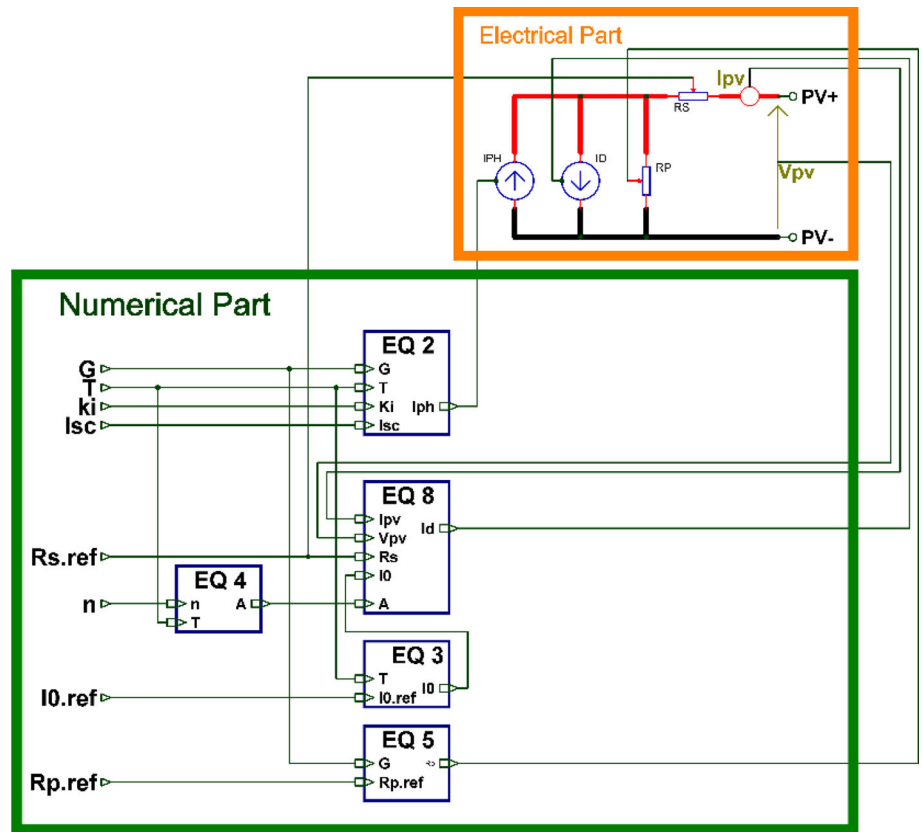
Table 1 Manufactures’ parameters at STC

Parameter	Signification	Unit
G	PV module absorbed solar irradiance	$[W/m^2]$
T	PV module temperature	$[^{\circ}C]$
k_i	Short-circuit temperature coefficient	$[mA/^{\circ}C]$
I_{sc}	PV module short-circuit current	$[A]$
n	Diode ideality factor	/
N_s	Number of series cells	/
N_p	Number of parallel cells	/
E_g	Gap energy at STC	$[eV]$
I_{0-ref}	Reverse saturation Current at STC	$[A]$
R_{s-ref}	Series resistance at STC	$[\Omega]$
R_{p-ref}	Parallel resistance at STC	$[\Omega]$

4 Simulation results and discussion

To assess the accuracy of the proposed PV model in ISIS-Proteus software, a comparative simulation study is conducted. In this study, the performance of the proposed model considering I–V and P–V characteristics is investigated under UTCs with varying irradiance and temperature and PSCs. In addition, I–V and P–V characteristics obtained from PVsyst software data and real data collected from a large-scale grid-connected PV station located in Ain El-Melh, Algeria, are considered for comparison. Furthermore, well-known statistical metrics, including the mean absolute error (MBE), determination coefficient (R^2), and relative errors (ξ) for critical points of the I–V curve (short-circuit, open-circuit, and MPPs), are considered to evaluate the model characteristics. The expressions of these statistical metrics are:

Fig. 5 Block diagram of the proposed new model of the PV module in ISIS-Proteus



$$R^2 = 1 - \frac{\sum_{i=1}^N (I_{i-s} - I_{i-m})^2}{\sum_{i=1}^N \left(I_{i-s} - \frac{1}{N} \sum_{i=1}^N I_{i-m} \right)^2} \tag{10}$$

$$MBE = 1 - \frac{1}{N} \sum_{i=1}^N (I_{i-s} - I_{i-m}) \tag{11}$$

$$\xi_{P_{max}} = \left| \frac{P_{sc-s} - P_{sc-m}}{P_{sc-s}} \right| \times 100 \tag{12}$$

$$\xi_{I_{sc}} = \left| \frac{I_{sc-s} - I_{sc-m}}{I_{sc-s}} \right| \times 100 \tag{13}$$

$$\xi_{V_{oc}} = \left| \frac{V_{oc-s} - V_{oc-m}}{V_{oc-s}} \right| \times 100 \tag{14}$$

where I_{i-s} and I_{i-m} denote the proposed model and PV_{sys} or real data currents at the i^{th} point, respectively, and N is the values' total number. Similarly, P_{max} , P_{max-m} , I_{sc-s} , I_{sc-m} , V_{oc-s} , and V_{oc-m} present the proposed model and PV_{sys} or real data maximum powers, short-circuit currents, and open-circuit voltages, respectively.

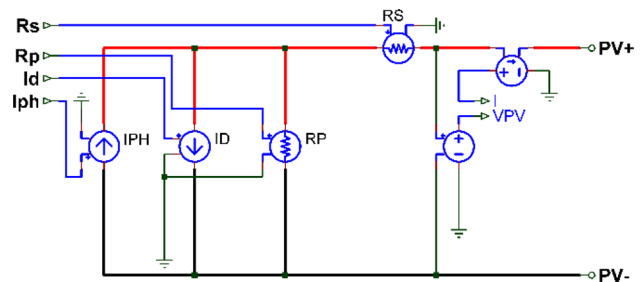


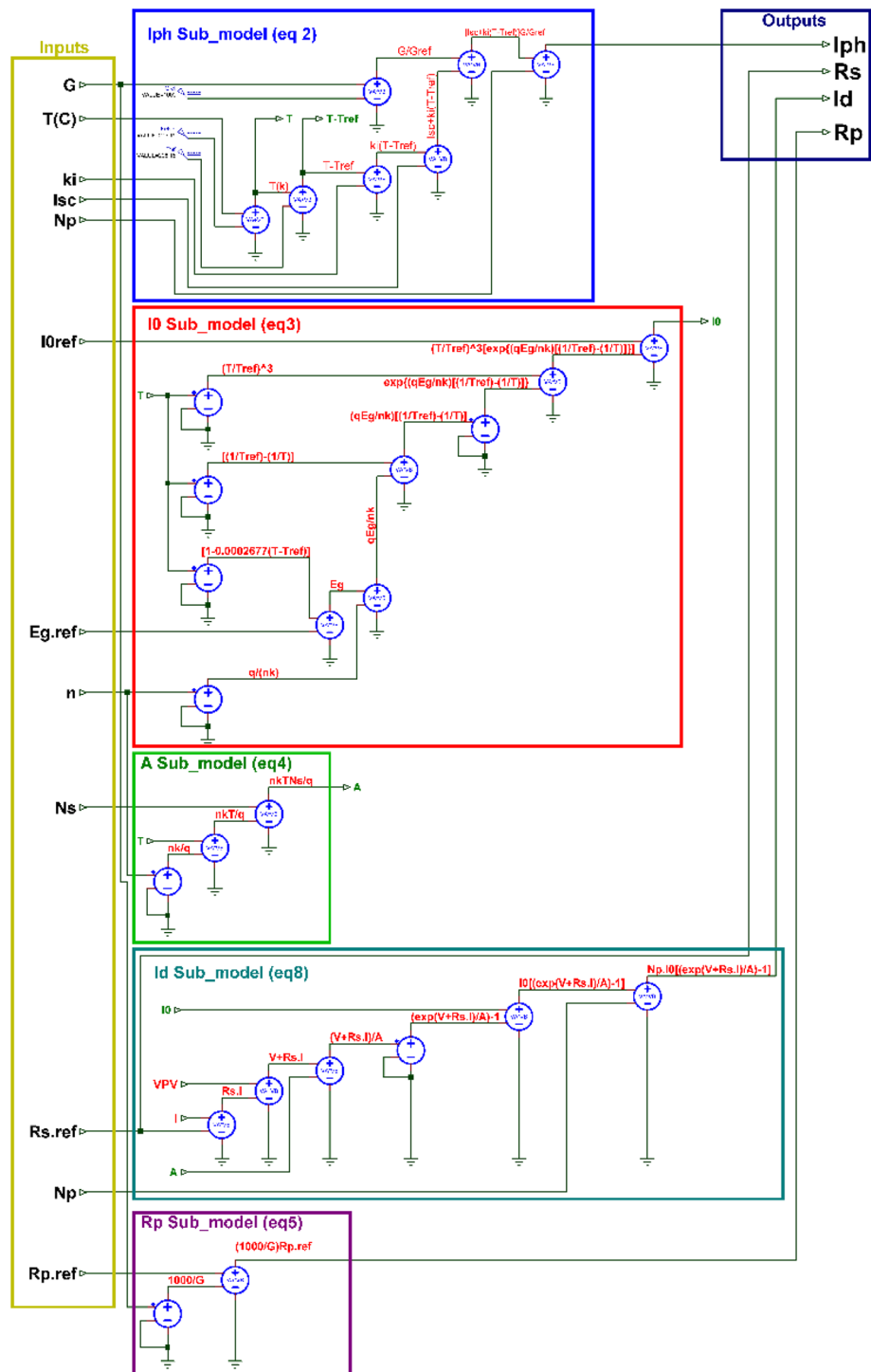
Fig. 6 Electric part of the proposed PV model implemented under ISIS-Proteus

4.1 Comparison with the PV_{sys} software

In this subsection, the proposed model's accuracy considering I–V and P–V characteristics is compared with the ones of the PV_{sys} software. In addition, the accuracy of the proposed model is tested under two cases; UTCs and PSCs.

1) Case 1: Accuracy assessment under UTCs: In this case, simulation tests are carried out using ISIS-Proteus to investigate the accuracy of the proposed model in comparison with PV_{sys} PV modules from three different technologies under UTCs. The types of PV modules are given below, with the specifications listed in Table 2, obtained based on the PV_{sys} software database.

Fig. 7 Numerical part of the proposed PV model implemented under ISIS-Proteus



- A silicon monocrystalline SHARP NU-180 (E1) PV module.
- A silicon polycrystalline Alex Solar ALP180-24 PV module.
- A silicon CIS Thin film Siemens_ST40.PAN PV module.

Note that the PV modules' specifications are brought from the manufacturer's data available in the PVsyst database, which ensures that the parameters and characteristics used in the analysis are based on reliable and standardized information provided by the manufacturer through the PVsyst. In addition, the parameters extracted from these modules under

Table 2 PV modules specifications

PV module type	SHARP NU-180 (E1)	Alex Solar ALP180-24	Siemens_ST40.PAN
Technology	Si-Mono	Si-Poly	CIS
Characteristics at STC	Value		
Maximum power (P_{max})	180 W	180 W	38 W
Voltage at P_{max} (V_{mp})	23,70 V	35, 30 V	16, 60 V
Current at P_{max} (I_{mp})	7,6 A	5,110 A	2,290 A
Short-circuit current (I_{sc})	8,37 A	5,32 A	2,590 A
Open-circuit voltage (V_{oc})	30,00 V	44,60 V	22,20 V
Temperature coefficient of open-circuit voltage (K_v)	- 48 m V/°C	- 139 m V/°C	- 84 m V/°C
Temperature coefficient of short-circuit current (K_i)	4,43 m A/°C	2,6 m A/°C	1,2 m A/°C
Number of cells in series (N_s)	48	72	42
The number of cells in parallel (N_p)	1	1	1
Diode saturation current (I_{0-ref})	$3,47e^{-9}$ A	$1,8e^{-9}$ A	$0,28635e^{-9}$ A
Diode ideality factor (A_{ref})	1,128	1,128	1,287
Parallel resistance (R_{p-ref})	150 Ω	850 Ω	300 Ω
Series resistance (R_{s-ref})	0.35 Ω	0.57 Ω	1.033 Ω

UTCs are reported in the Proteus tool, enabling the construction of model curves for visual representation.

The obtained results presenting the I–V and P–V characteristics in response to two different values of irradiance and temperature are portrayed in Figs. 8, 9, 10 for SHARP NU-180 (E1), Alex Solar ALP180-24, Siemens_ST40.PAN PV module types, respectively. From these figures, it can be seen that the I–V and P–V curves achieved by the proposed model in ISIS-Proteus are matched with the PVsyst ones. However, a tinny error is remarked in the P–V characteristics of the SHARP NU-180 (E1) PV module (see Fig. 8a) for the case of $G = 795,6 \text{ W/m}^2$ and $T = 30,55 \text{ }^\circ\text{C}$. These observations are confirmed through the numerical findings reported in Table 3, which highlights that for the different PV modules operating under the irradiance and temperature amounts:

- The numerical values of all the parameters are very close,
- The determination coefficient (R^2) is almost equal to 1, which means that the I–V and P–V curves of the two models are matched.
- The MBE and the relative errors have very small values.

Therefore, it can be concluded that the proposed model is quite accurate under UTCs compared to the PVsyst models.

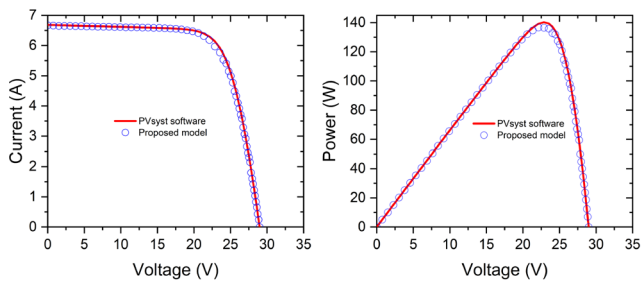
2) Case 2: Accuracy assessment under PSCs: Here, the proposed model accuracy is investigated under PSCs in comparison with a PVsyst model considering Isofoton I_106/24 PV module type with specifications listed in Table 4, which

are taken from the manufacturer's data available in the PVsyst database. Figure 11 shows the simulation model implemented in ISIS-Proteus, which is a string, composed of three proposed models of Isofoton I_106/24 PV module type. In this string, each PV module is subjected to different solar irradiance levels, 1000 W/m^2 , 700 W/m^2 , and 300 W/m^2 . The current at each level is limited by the short-circuit current of each PV module based on the solar irradiance level. This short-circuit current is split into three levels; 3.097 A at 1000 W/m^2 , 2.201 A at 700 W/m^2 , and 0.951 A at 300 W/m^2 .

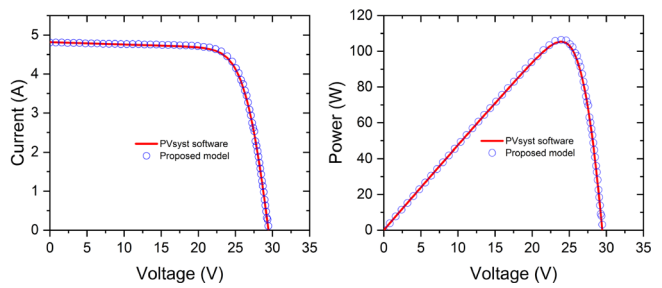
The resulting I–V and P–V curves of the two models under the PSCs are illustrated in Fig. 12. While Table 5 presents the comparison numerical findings highlighting the PV module climatic parameters and the relative error of P_{max} for each radiation level. The results show a close agreement between the curves and parameters of the proposed model and the PVsyst model with a very small relative error. This indicates the accuracy of the proposed model in capturing the behavior of the PV string under PS.

4.2 Comparison with real data

This subsection investigates the accuracy assessment of the proposed model is compared to I–V and P–V curves achieved through real data collected from Ain-Elmelh station under UTCs and PSCs using ISIS-Proteus software. In this test, a PV module type Yingli solar 250 Wp is considered with the specifications at STCs presented in Table 6. The real data



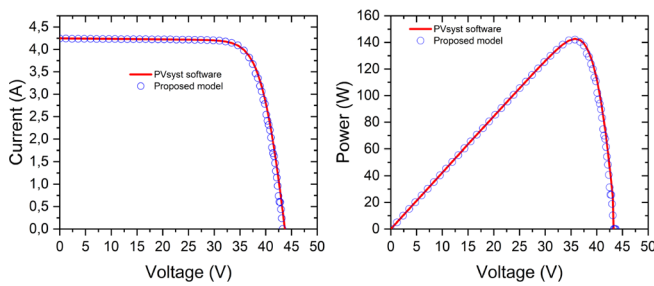
(a) I-V and P-V characteristics of the proposed model and PVsyst model for $G = 795,6 \text{ W/m}^2$ and $T = 30,55 \text{ }^\circ\text{C}$ (SHARP NU 180 E1 PV module)



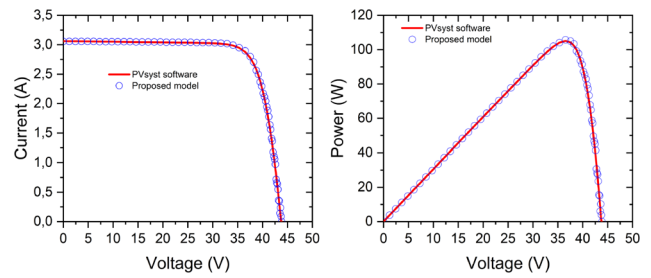
(a) I-V and P-V characteristics of the proposed model and PVsyst model for $G = 575 \text{ W/m}^2$ and $T = 23,26 \text{ }^\circ\text{C}$ (SHARP NU 180 E1 PV module)

Fig. 8 **a** I-V and P-V characteristics of the proposed model and PVsyst model for $G = 795,6 \text{ W/m}^2$ and $T = 30,55 \text{ }^\circ\text{C}$ (SHARP NU-180 E1 PV module). **b** I-V and P-V characteristics of the proposed model and

PVsyst model for $G = 575 \text{ W/m}^2$ and $T = 23,26 \text{ }^\circ\text{C}$ (SHARP NU-180 E1 PV module)

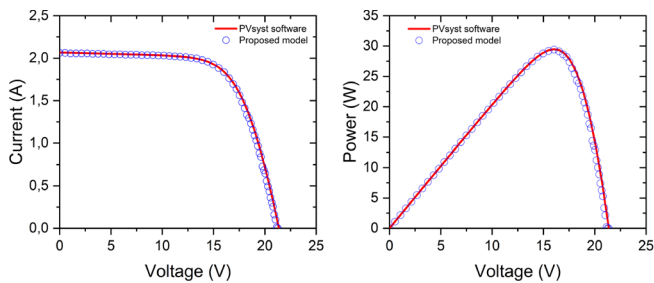


(a) I-V and P-V characteristics of the proposed model and PVsyst model for $G = 795,6 \text{ W/m}^2$ and $T = 30,55 \text{ }^\circ\text{C}$ (ALP180-24 PV module)

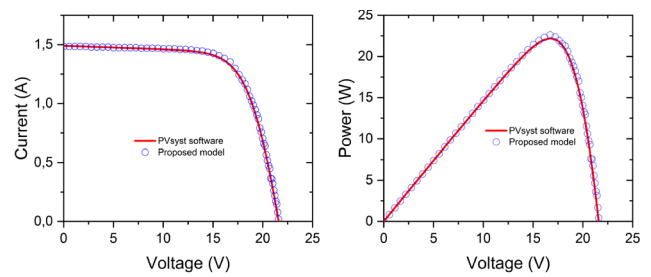


(b) I-V and P-V characteristics of the proposed model and PVsyst model for $G = 575 \text{ W/m}^2$ and $T = 23,26 \text{ }^\circ\text{C}$ (ALP180-24 PV module)

Fig. 9 **a** I-V and P-V characteristics of the proposed model and PVsyst model for $G = 795,6 \text{ W/m}^2$ and $T = 30,55 \text{ }^\circ\text{C}$ (ALP180-24 PV module). **b** I-V and P-V characteristics of the proposed model and PVsyst model for $G = 575 \text{ W/m}^2$ and $T = 23,26 \text{ }^\circ\text{C}$ (ALP180-24 PV module)



(a) I-V and P-V characteristics of the proposed model and PVsyst model for $G = 795,6 \text{ W/m}^2$ and $T = 30,55 \text{ }^\circ\text{C}$ (Siemens_ST40.PAN)



(b) I-V and P-V characteristics of the proposed model and PVsyst model for $G = 575 \text{ W/m}^2$ and $T = 23,26 \text{ }^\circ\text{C}$ (Siemens_ST40.PAN)

Fig. 10 **a** I-V and P-V characteristics of the proposed model and PVsyst model for $G = 795,6 \text{ W/m}^2$ and $T = 30,55 \text{ }^\circ\text{C}$ (Siemens_ST40.PAN). **b** I-V and P-V characteristics of the proposed model and PVsyst model for $G = 575 \text{ W/m}^2$ and $T = 23,26 \text{ }^\circ\text{C}$ (Siemens_ST40.PAN)

Table 3 Results and metrics of the comparison under UTCs

PV module type		SHARP NU-180 E1		ALP180-24		Siemens_ST40.PAN	
Solar irradiance	$G \text{ W/m}^2$	795,6	575,58	795,6	575,58	795,6	575,58
Cell temperature	$T \text{ (}^\circ\text{C)}$	30,55	23,26	30,55	23,26	30,55	23,26
PVsyst model parameters	$I_{sc,m} \text{ (A)}$	6,6840	4,8172	4,2470	3,0616	2,0675	1,4910
	$V_{oc,m} \text{ (V)}$	28,9811	29,448	43,7050	43,7349	21,3650	21,5862
	$P_{max,m} \text{ (W)}$	140,3061	105,4881	142,7275	105,1211	29,4780	22,2032
Proposed model parameters	$I_{sc,s} \text{ (A)}$	6,6700	4,805	4,2430	3,0570	2,0610	1,4840
	$V_{oc,s} \text{ (V)}$	29,2480	29,492	43,2713	43,8477	21,2541	21,6553
	$P_{max,s} \text{ (W)}$	136,6995	106,4249	142,1838	105,7822	29,4219	22,6093
Value Metrics	R^2	0,9989	0,9991	0,9888	0,9984	0,9961	0,9981
	MBE	0,0475	0,0339	0,0836	0,0164	0,0294	0,0147
	$\xi_{Isc} \text{ (%)}$	0,2099	0,2539	0,0943	0,1505	0,3154	0,4717
	$\xi_{Voc} \text{ (%)}$	0,9125	0,1492	1,0023	0,2573	0,5148	0,3191
	$\xi_{Pmax} \text{ (%)}$	2,6384	0,8803	0,3824	0,6250	0,1906	1,7960

are collected considering the experimental setup depicted in Fig. 13, which is built using commercial PV modules installed in a large-scale grid-connected PV station located in Ain El-Melh, Algeria. The components used in the experimental setup are listed hereafter:

- Yingli YL250P (250Wp) PV module;
- I–V characteristics tracer type Kewell IVT-12–1000;
- In-plane irradiance sensor (Pyranometer type: KIPP&ZONEM);
Cell temperature sensor (Pt1000).

Similar to the previous subsection, the proposed model undergoes assessment across two case studies; under UTCs and PSCs.

- 1) **Case 1: Accuracy assessment under UTCs:** In this case, the models’ accuracy is tested under UTCs considering two scenarios; a single Yingli YL250 PV module and a PV string of 22 PV Yingli YL250 modules.
- A. **Scenario 01:** Figure 14 shows the simulation model conducted in ISIS-Proteus based on a single Yingli YL250 PV module. The obtained results showing the I–V and P–V curves of the proposed model and of the real data, for two different values of irradiance and temperature are presented in Figs. 15 and 16, respectively. As can be seen, the model exhibits good agreement with the real data. In addition, the relative errors of I_{sc} , V_{oc} , and P_{max} are found around 0.17%, 1.08%, and 1.22% for $G = 885 \text{ W/m}^2$ and $T = 60^\circ\text{C}$, and 0.22%, 1.59%, and 0.84% for $G = 668 \text{ W/m}^2$ and $T = 51^\circ\text{C}$. Furthermore, the mean

Table 4 Isofoton I_106/24 specifications

PV module type	Isofoton I_106 / 24
Technology	Si-Mono
Characteristics at STC	Value
Maximum power (P_{max})	106 W
Voltage at P_{max} (V_{mp})	34,80 V
Current at P_{max} (I_{mp})	3,05 A
Short-Circuit current (I_{sc})	3,27 A
Open-circuit voltage (V_{oc})	43,60 V
Temperature coefficient of open-circuit voltage (K_v)	• - 142 mV/°C
Temperature coefficient of short-circuit current (K_i)	2,3 mA/°C
The number of cells in series (N_s)	72
Number of cells in parallel (N_p)	1
Diode saturation current (I_0)	0,24e-9 A
Diode ideality factor (A_{ref})	1,010
Parallel resistance (R_{p-ref})	800 Ω
Series resistance (R_{s-ref})	1,11 Ω

absolute error (MAE) and the coefficient of determination are obtained about 0.28 and 0.82 for $G = 885 \text{ W/m}^2$ and $T = 60^\circ\text{C}$, and 0.19 and 0.79 for $G = 668 \text{ W/m}^2$ and $T = 51^\circ\text{C}$. These metrics highlight that the proposed model can predict the behavior of the real module with high accuracy under this specific condition.

Scenario 02: Here, a simulation model built based on a PV string comprising 22 series-connected modules

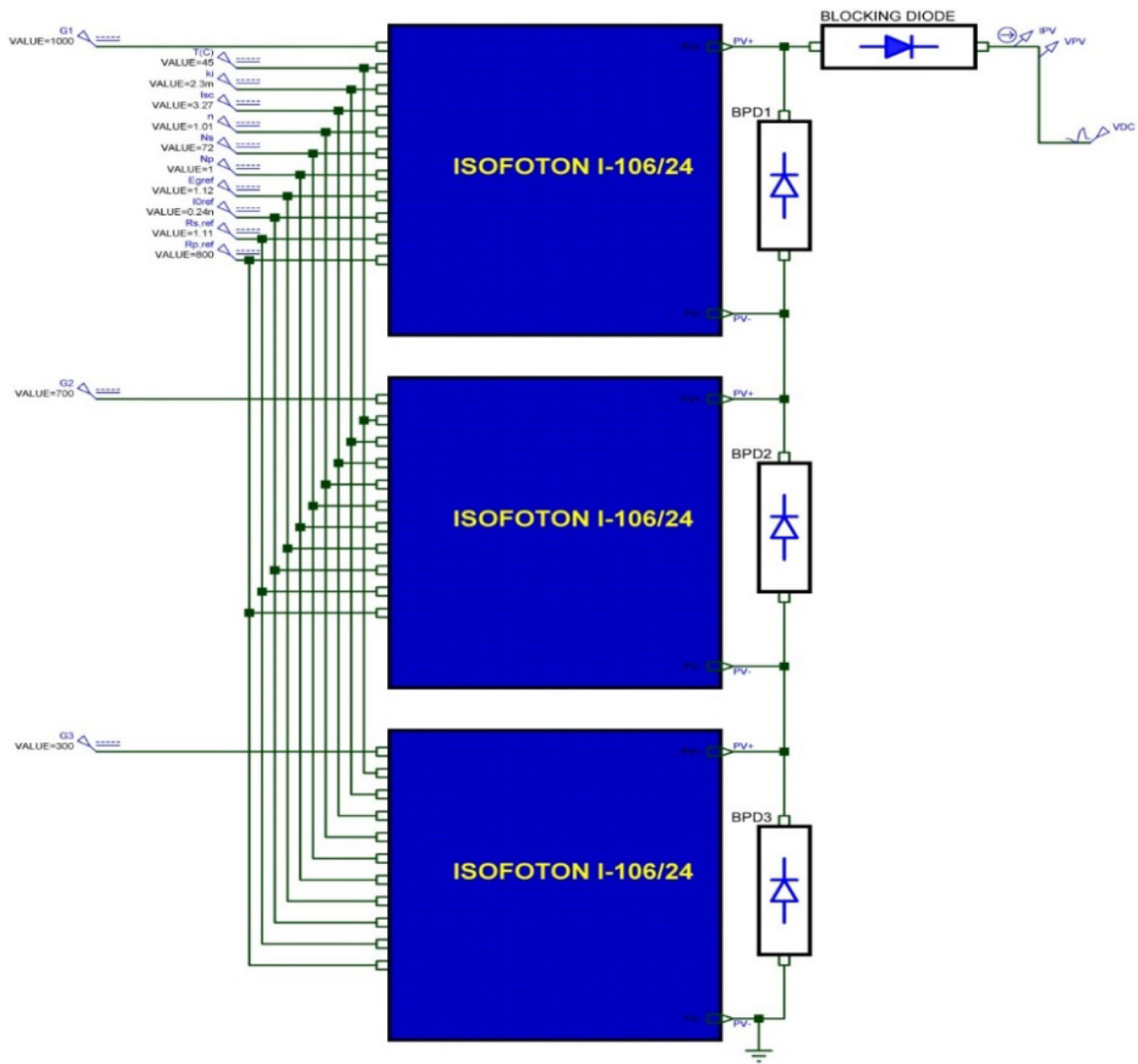


Fig. 11 Implemented simulation model using ISIS-Proteus of a string consisting of 3 proposed PV Isofoton I_106/24 type modules

Fig. 12 Accuracy assessment under PS for different radiation levels; $G = 1000\text{W/m}^2$, $G = 700\text{W/m}^2$, and $G = 300\text{W/m}^2$ with $T = 45\text{ }^\circ\text{C}$

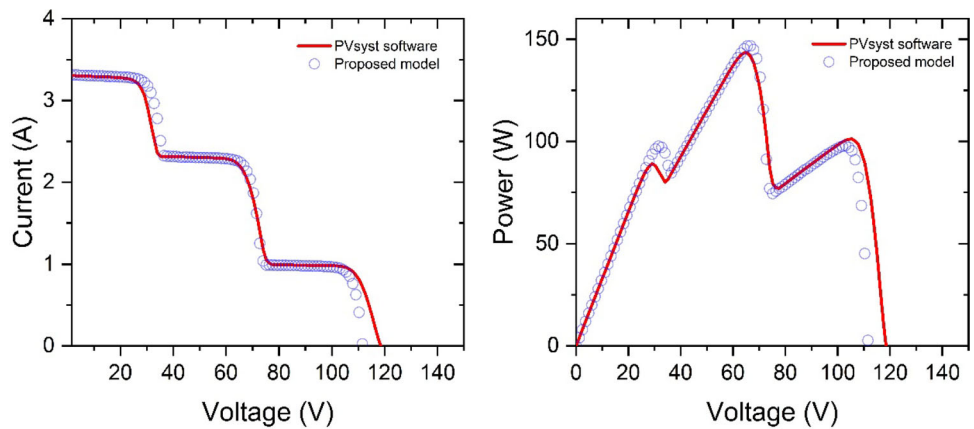


Table 5 Results of the comparison study under PSCs

Climatic parameters	Symbols	Value	Value	Value
Solar irradiance	G W/m ²	1000	700	300
Cell temperature	T(°C)	45		
<i>Module characteristic parameters</i>				
PV String Zones		LMPP1	GMPP	LMPP2
PVsyst model	I _{sc,m} (A)	3.097	2.201	0,951
	P _{max,m} (W)	97,7766	146,81	97,9887
Proposed model	I _{sc,s} (A)	3,3110	3.30	0,9912
	P _{max,s} (W)	92,2519	143,34	102,1286
Value				
Relative error	ε _{Pmax} (%)	14.25	2.41	2.56

Table 6 YINGLI SOLAR YL2545-29B PV Module Specification

Parameter	Value
STC rating power (P_{max})	250 Wp ± 5%
Number of cells (N_s)	60
V_{mp}	29.8 V
I_{sc}	8.92 A
I_{mp}	8.39 A
V_{oc}	37.6 V
Power temperature coefficient K_p (%/°C)	B. - 0.45
NOCT (°C)	1000 V

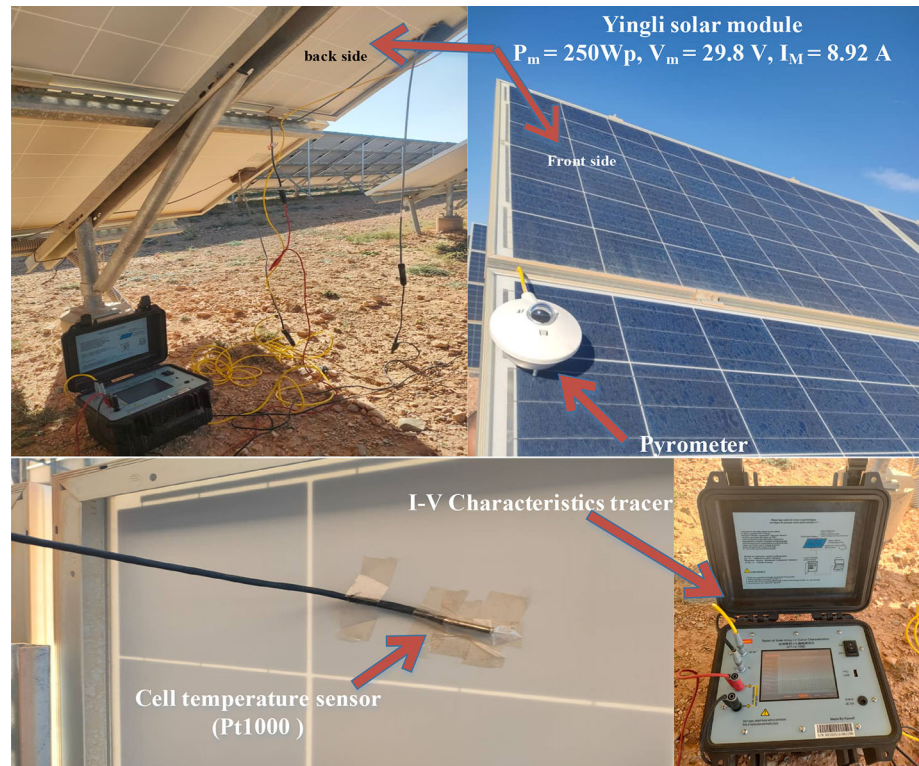
is used for the accuracy investigation of the proposed model under UTCs. The Yingli YL250P PV module string simulated using ISIS-Proteus and implemented in the real world for data collection is depicted in Fig. 17a and b. Note that such a comparison between simulation and actual implementation facilitates the evaluation of the PV system’s performance and accuracy in practical conditions. The achieved I–V and P–V curves of the proposed model compared to real data under various values of irradiance and temperature are shown in Figs. 18, 19, 20, 21, 22, 23. From these figures, it can be noticed that the proposed model curves closely match the curves of the real data for the different irradiance and temperature levels. This agreement is validated via the numerical findings reported in Table 7. As a consequence, the proposed ISIS-Proteus model demonstrates high precision in predicting the behavior of the real PV module under extreme UTCs.

2) **Case 2: Accuracy assessment under PSCs:** This case presents the accuracy investigation of the proposed model under various PSCs in comparison with real data. Similarly, two scenarios are considered; a single Yingli YL250 PV module and a PV string consisting of four series-connected PV Yingli YL250 modules.

A. **Scenario 01:** This part examines the accuracy of the proposed PV module model of a single PV module under various PSCs. Figure 24 shows the implemented PV module in ISIS-Proteus software, which is configured based on three bypass diodes resembling three sub-modules in series. The resulting I–V and P–V curves are depicted in Fig. 25b and c for $G = 890$ W/m² and $T = 61$ °C with shading in the lower third part of the real-world PV module, as Fig. 25a shows. These results highlight acceptable agreement of the proposed model with real data. In addition, the achieved relative errors of I_{sc} , V_{oc} , and P_{max} around 2.4%, 0.62%, and 8.43%, respectively, confirmed this agreement. Furthermore, this agreement is also verified through the slightly obtained values of the MAE and R^2 of about 1.23 and 0.45, respectively.

B. **Scenario 02:** Under this scenario, the proposed model accuracy is verified considering a PV string of 4 PV modules working against various PSCs. The real-world PV modules and the simulated PV string model in ISIS-Proteus software are shown in Fig. 26. The obtained results for two different values of irradiance and temperature are illustrated in Figs. 27 and 28 corresponding to specified PS. The I–V and P–V curves of Figs. 27b and c are obtained for a shading affecting modules 1 and 2, shown in Fig. 27a, and for $G = 849$ W/m² and $T = 38$ °C. However, Fig. 28b and c portrays the I–V and P–V curves for a shade that affects modules 1, 2, and 4, shown in Fig. 28a, and for $G = 857$ W/m² and $T = 37$ °C. According to these figures, it can be observed that the proposed model exhibited good agreement with the real model. This agreement is validated regarding the obtained slight relative errors of I_{sc} , V_{sc} , and P_{max} (0.82% 4.05%, 5.39% for the first test, and 0.15%, 4.08%, 5.39% for the second test), as well as the found values of the MAE and R^2 (0.82% and 5.39% for the first test, and 0.04%, 0.99% for the second test).

Fig. 13 Experimental setup with components



Overall, the obtained results validate the accuracy of the proposed model of the PV module implemented using ISIS-Proteus versus the real models under various PSCs.

5 Conclusion

In this paper, the implementation of a new PV module model in an ISIS-Proteus environment suitable for both UTCs and PSCs was presented. Different simulation tests were conducted in ISIS-Proteus software to assess the accuracy of the proposed model in comparison with PVsyst software models and real data brought from Ain El-Melh station in Algeria under various UTCs and PSCs. In the first test, the proposed model's performance was compared to the PVsyst model considering three types of PV modules, SHARP NU-180, Alex Solar ALP180-24, and Siemens ST40.PAN, under two different levels of irradiance and temperature. The second test was focused on examining the accuracy of the designed model under varying shading levels in comparison with the PVsyst model based on a PV string with three Isofoton I_106/24 modules. The results revealed high accuracy in predicting the behavior of the PVsyst PV module/string, with maximum relative errors around 0,47% for short-circuit current, 1% for open-circuit voltage, and 2,64% for maximum power under and high correlation close to 1 under UTCs, and maximum relative error of power about 5,99% under PSCs. The third test, which evaluated the accuracy of the proposed

PV model, is a comparison with real data under varying irradiance and temperature conditions considering a single and string of 22 Yingli YL250 PV modules, the results demonstrated that the proposed model has good accuracy. More particular, the model, in the case of a string, exhibited a high correlation with real data, the minimum amount was for $G = 1047 \text{ W/m}^2$ and $T = 48 \text{ }^\circ\text{C}$, and very small relative errors with maximum values of 1.71% for short-circuit current, 3.65% for open-circuit voltage, and 3.6% for maximum power. The results of the fourth test, that investigated the model accuracy under PSCs for also a single and a string of 4 Yingli YL250 PV modules, showed acceptable performance. The single module model offered errors of short-circuit current and maximum power around 2.4% and 8.43%, while the string model exhibited lower relative errors of 0.15% for short-circuit current and 5.39% maximum power. These findings validated the effectiveness of the proposed model in predicting PV system behavior with accuracy under various UTCs and PSCs, closely aligning with real-world performance. In future work, we plan to create a model that simulates the degradation of photovoltaic modules over time, considering environmental factors and material fatigue. This will help predict long-term performance and optimize maintenance, enhancing PV system reliability and efficiency.

Fig. 14 ISIS-Proteus simulation model for scenario 01

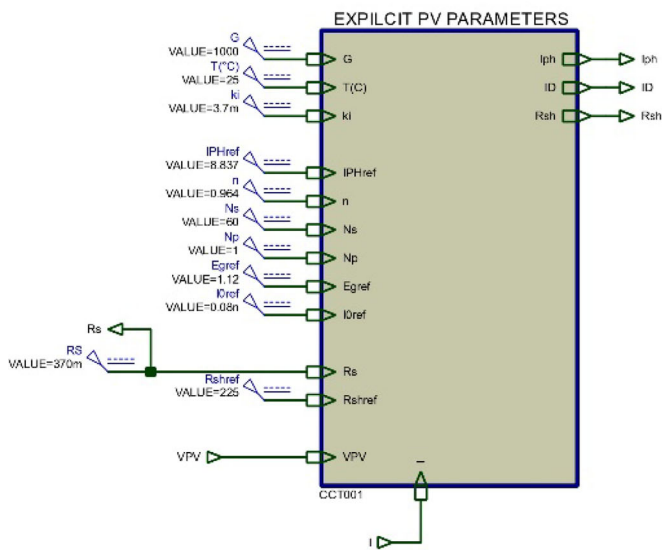
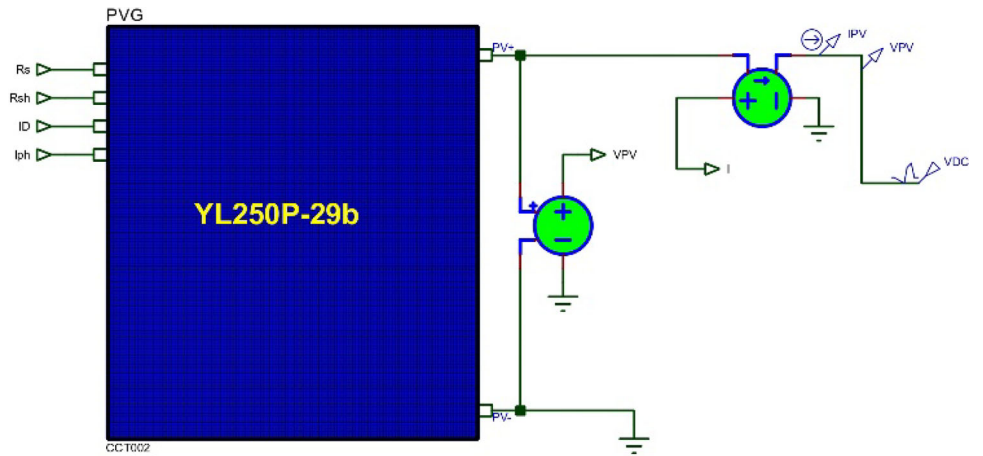


Fig. 15 Results of scenario 01 for $G = 885 \text{ W/m}^2$ and $T = 62 \text{ }^\circ\text{C}$; **a** I-V curve and **b** P-V curve

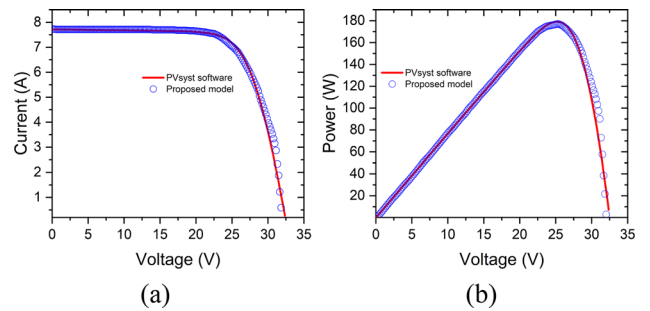
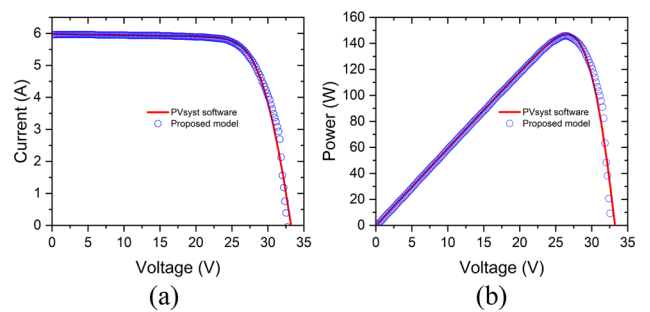
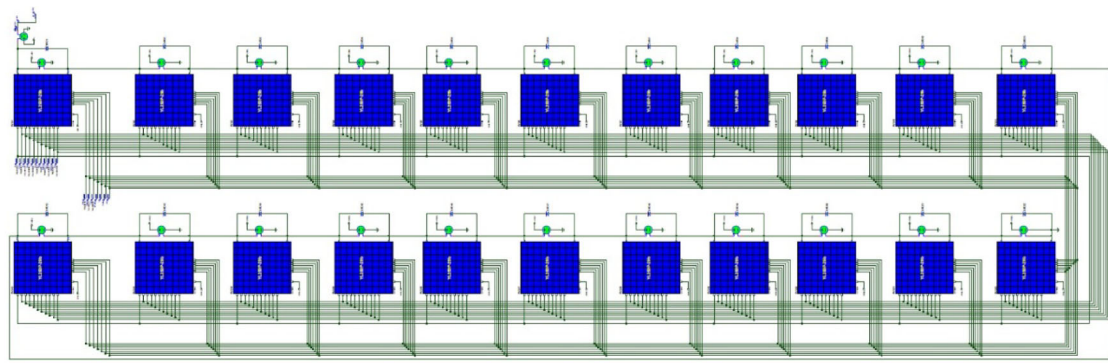


Fig. 16 Results of scenario 01 for $G = 668 \text{ W/m}^2$ and $T = 51 \text{ }^\circ\text{C}$; **a** I-V curve and **b** P-V curve





(a)



(b)

Fig. 17 PV string comprising 22 series-connected modules for **a** ISIS-Proteus simulation, and **b** real-world implementation

Fig. 18 Results of scenario 02 for $G = 262 \text{ W/m}^2$ and $T = 30 \text{ }^\circ\text{C}$; **a** I-V curve and **b** P-V curve

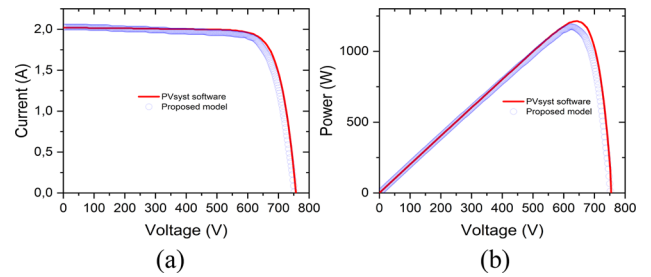


Fig. 19 Results of scenario 02 for $G = 386 \text{ W/m}^2$ and $T = 34 \text{ }^\circ\text{C}$; **a** I-V curve and **b** P-V curve

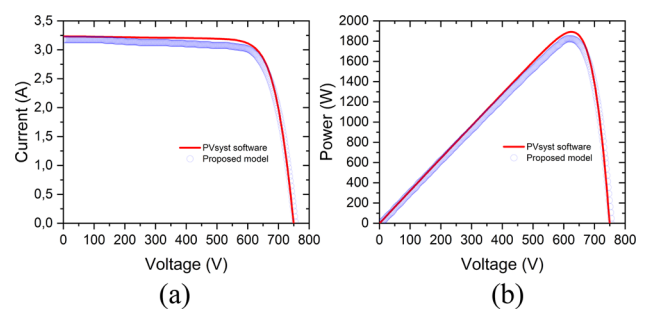


Fig. 20 Results of scenario 02 for $G = 525 \text{ W/m}^2$ and $T = 38 \text{ }^\circ\text{C}$; **a** I–V curve and **b** P–V curve

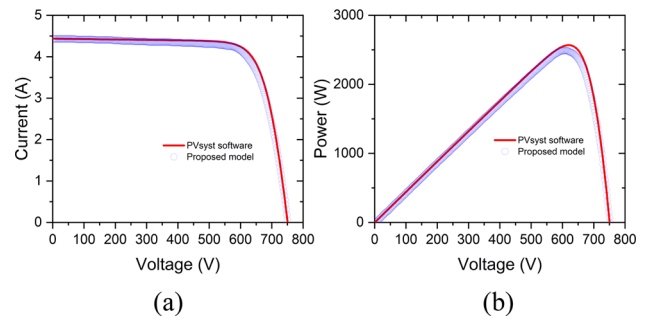


Fig. 21 Results of scenario 02 for $G = 715 \text{ W/m}^2$ and $T = 45 \text{ }^\circ\text{C}$; **a** I–V curve and **b** P–V curve

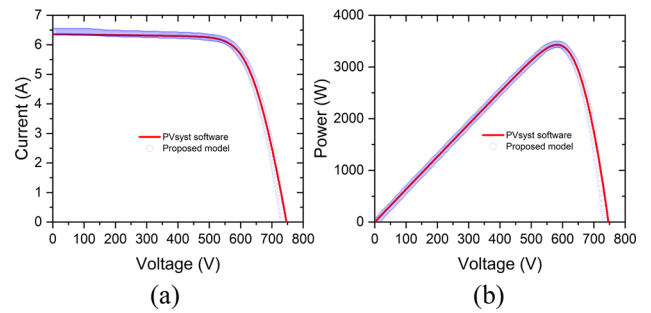


Fig. 22 Results of scenario 02 for $G = 969 \text{ W/m}^2$ and $T = 47 \text{ }^\circ\text{C}$; **a** I–V curve and **b** P–V curve

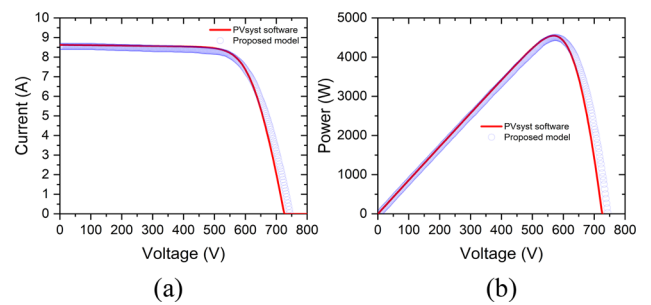


Fig. 23 Results of scenario 02 for $G = 1047 \text{ W/m}^2$ and $T = 48 \text{ }^\circ\text{C}$; **a** I–V curve and **b** P–V curve

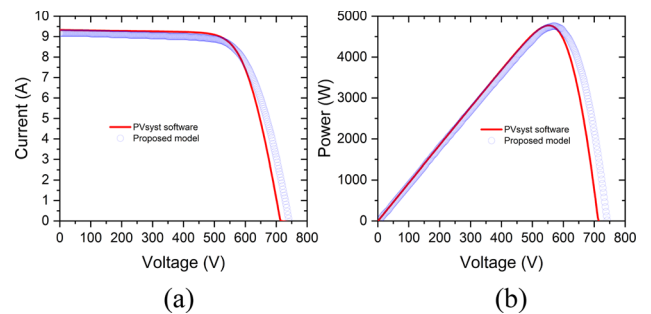


Table 7 Results of the comparison study for scenario 02

Solar irradiance	$G \text{ W/m}^2$	262 W/m^2	386 W/m^2	525 W/m^2	715 W/m^2	969 W/m^2	1047 W/m^2
Temperature	$T \text{ (}^\circ\text{C)}$	30 $^\circ\text{C}$	34 $^\circ\text{C}$	38 $^\circ\text{C}$	45 $^\circ\text{C}$	47 $^\circ\text{C}$	48 $^\circ\text{C}$
Metrics	R^2	0.99	0.99	0.997	0.976	0.92	0.91
	MBE	0.04	0.05	0.08	0.07	0.12	0.08
	$\xi_{Isc} \text{ (%)}$	0.41%	1.71%	0.15%	1.39%	0.91%	1.63%
	$\xi_{Voc} \text{ (%)}$	0.53%	0.8%	0.23%	1.34%	2.48%	3.65%
	$\xi_{Pmax} \text{ (%)}$	3.53%	3.6%	2.94%	0.22%	1.03%	0.18%

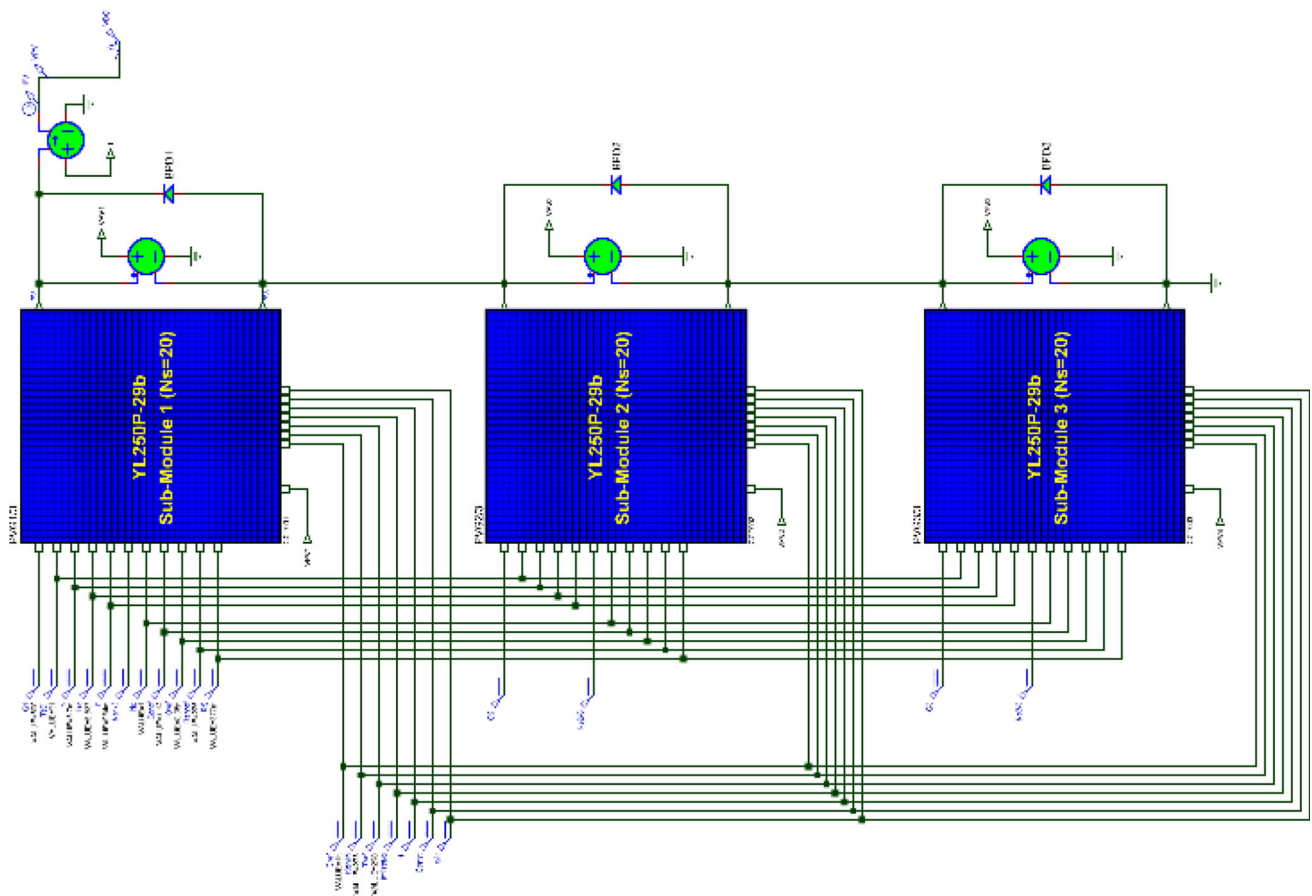


Fig. 24 Simulated Yingli YL250P PV module in ISIS-Proteus consists of three sub-modules with three bypass diodes

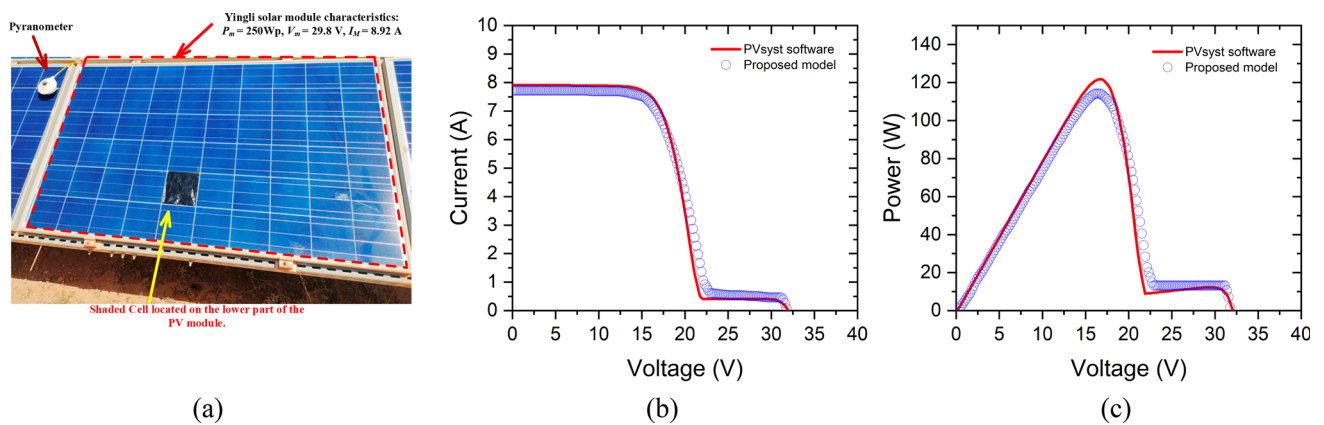


Fig. 25 a Real-world PV module under shade, and results of scenarios 01 under PSCs for $G = 890\text{ W/m}^2$ and $T = 61\text{ }^\circ\text{C}$; b I–V curve and c P–V curve

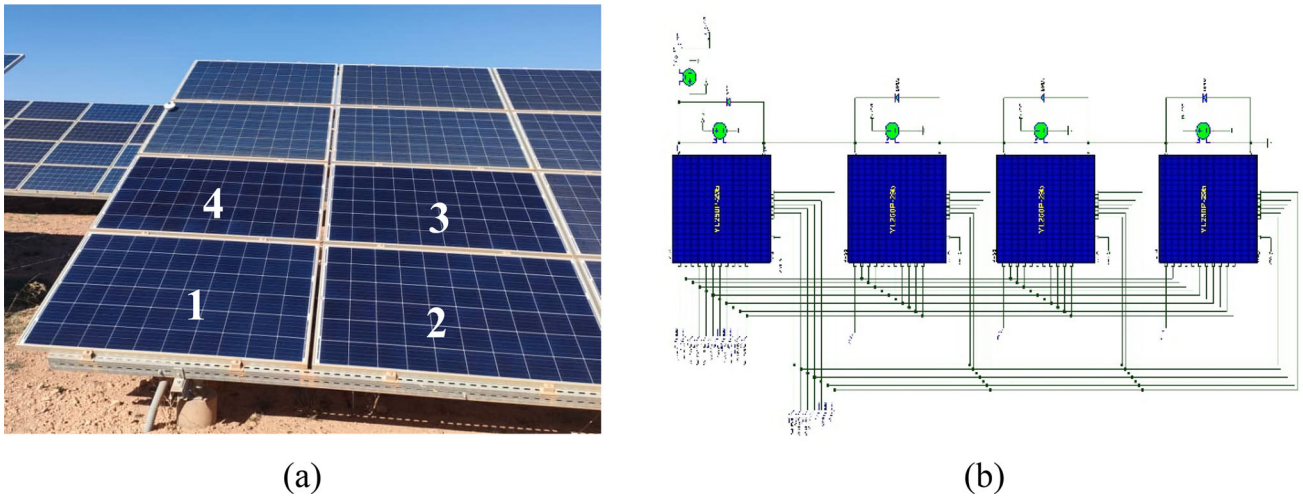


Fig. 26 Configuration of a PV string comprising four series-connected modules; **a** real-world and **b** implemented model simulation in ISIS-Proteus

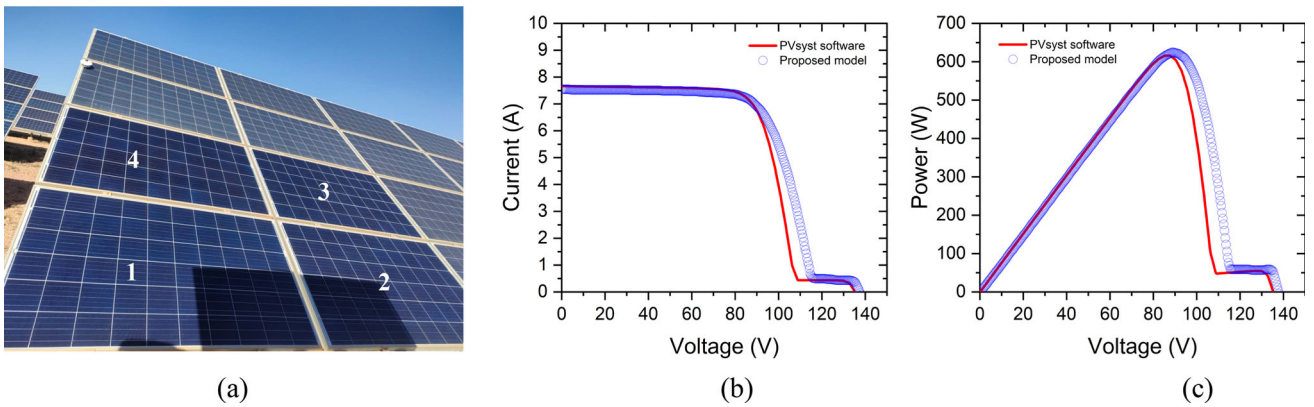


Fig. 27 **a** Real-world PV module under shade, and results of scenarios 02 under PSCs for $G = 849 \text{ W/m}^2$ and $T = 38 \text{ }^\circ\text{C}$; **b** I–V curve and **c** P–V curve

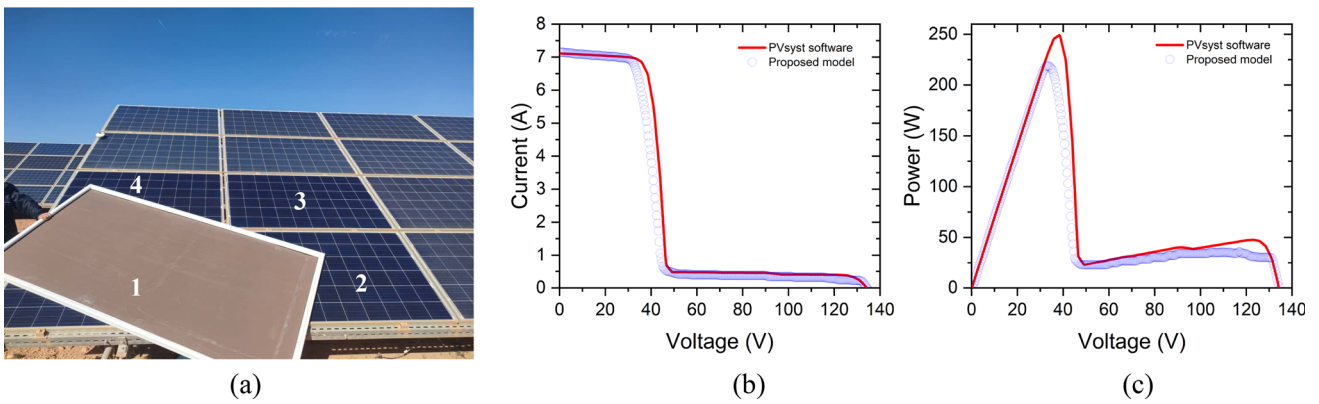


Fig. 28 **a** Real-world PV module under shade, and results of scenarios 02 under PSCs for $G = 857 \text{ W/m}^2$ and $T = 37 \text{ }^\circ\text{C}$; **b** I–V curve and **c** P–V curve

Acknowledgements The authors gratefully acknowledge the Algerian General Direction of Research (DGRSDT) for providing the facilities and the financial funding of this project.

Author's contribution AL was involved in conceptualization, investigation, methodology, writing—review and editing. AAA helped in formal analysis, investigation, methodology, validation, writing—original draft. DS contributed to formal analysis, investigation, methodology, validation, writing—original draft. MD was involved in conceptualization, supervision, writing—review and editing. AB provided real data and assisted in investigation, methodology, writing—review and editing. MK provided real data and helped in investigation, writing—review and editing.

Data availability No datasets were generated or analyzed during the current study.

Declarations

Conflict of interest The authors declare no competing interests.

References

- Loukriz A et al (2021) A new simplified algorithm for real-time power optimization of TCT interconnected PV array under any mismatch conditions. *J Eur des Syst Autom* 54(6):805–817. <https://doi.org/10.18280/jesa.540602>
- Bollipo RB, Mikkili S, Bonthagorla PK (2020) Hybrid, optimization, intelligent and classical PV MPPT techniques: review. *CSEE J Power Energy Syst*. <https://doi.org/10.17775/CSEEJPES.2019.02720>
- Zhu L, Li Q, Chen M, Cao K, Sun Y (2019) A simplified mathematical model for power output predicting of Building Integrated Photovoltaic under partial shading conditions. *Energy Convers Manag* 180:831–843. <https://doi.org/10.1016/j.enconman.2018.11.036>
- Adawi I (1964) Theory of the surface photoelectric effect for one and two photons. *Phys Rev* 134(3A):A788–A798. <https://doi.org/10.1103/PhysRev.134.A788>
- Walker G (2001) Evaluating MPPT converter topologies using a Matlab PV model. *J Electr Electron Eng Aust*
- Li Q, Zhu L, Sun Y, Lu L, Yang Y (2020) Performance prediction of Building Integrated Photovoltaics under no-shading, shading, and masking conditions using a multi-physics model. *Energy* 213:118795. <https://doi.org/10.1016/j.energy.2020.118795>
- Muhammadsharif FF et al. (2019) Brent's algorithm-based new computational approach for accurate determination of single-diode model parameters to simulate solar cells and modules. *Sol Energy* 193:782–798. <https://doi.org/10.1016/j.solener.2019.09.096>
- Keevers MJ, Green MA (1994) Efficiency improvements of silicon solar cells by the impurity photovoltaic effect. *J Appl Phys*. <https://doi.org/10.1063/1.356025>
- V. Lo Brano, A. Orioli, G. Ciulla, and A. Di Gangi (2010) An improved five-parameter model for photovoltaic modules. *Sol Energy Mater Sol Cells*. <https://doi.org/10.1016/j.solmat.2010.04.003>.
- Anani N, Ibrahim H (2020) Adjusting the single-diode model parameters of a photovoltaic module with irradiance and temperature. *Energies* 13(12):3226. <https://doi.org/10.3390/en13123226>
- Bouraiou A, Hamouda M, Chaker A, Sadok M, Mostefaoui M, Lachtar S (2015) Modeling and simulation of photovoltaic module and array based on one and two diode model using matlab/simulink. *Energy Proc*. <https://doi.org/10.1016/j.egypro.2015.07.822>
- G. Ciulla, V. Lo Brano, V. Di Dio, and G. Cipriani, 2014. A comparison of different one-diode models for the representation of I–V characteristic of a PV cell. *Renew Sustain Energy Rev* 32:684–696. <https://doi.org/10.1016/j.rser.2014.01.027>.
- Franzitta V, Orioli A, Di Gangi A (2016) Assessment of the usability and accuracy of the simplified one-diode models for photovoltaic modules. *Energies* 9(12):1019. <https://doi.org/10.3390/en9121019>
- Hovinen A (1994) Fitting of the solar cell IV -curve to the two diode model. *Phys Scr T54*:175–176. <https://doi.org/10.1088/0031-8949/1994/T54/043>
- Laudani A, Riganti Fulginei F, Salvini A (2014) Identification of the one-diode model for photovoltaic modules from datasheet values. *Sol Energy* 108:432–446. <https://doi.org/10.1016/j.solener.2014.07.024>.
- De Soto W, Klein SA, Beckman WA (2006) Improvement and validation of a model for photovoltaic array performance. *Sol Energy* 80(1):78–88. <https://doi.org/10.1016/j.solener.2005.06.010>
- Chatterjee A, Keyhani A, Kapoor D (2011) Identification of photovoltaic source models. *IEEE Trans Energy Convers* 26(3):883–889. <https://doi.org/10.1109/TEC.2011.2159268>
- Ma T, Yang H, Lu L (2014) Solar photovoltaic system modeling and performance prediction. *Renew Sustain Energy Rev* 36:304–315. <https://doi.org/10.1016/j.rser.2014.04.057>
- Ma T, Yang H, Lu L (2014) Development of a model to simulate the performance characteristics of crystalline silicon photovoltaic modules/strings/arrays. *Sol Energy* 100:31–41. <https://doi.org/10.1016/j.solener.2013.12.003>
- Ding K, Bian X, Liu H, Peng T (2012) A MATLAB-Simulink-based PV module model and its application under conditions of nonuniform irradiance. *IEEE Trans Energy Convers*. <https://doi.org/10.1109/TEC.2012.2216529>
- Yaqoob SJ, Saleh AL, Motahhir S, Agyekum EB, Nayyar A, Qureshi B (2021) Comparative study with practical validation of photovoltaic monocrystalline module for single and double diode models. *Sci Rep*. <https://doi.org/10.1038/s41598-021-98593-6>
- Nguyen XH, Nguyen MP (2015) Mathematical modeling of photovoltaic cell/module/arrays with tags in Matlab/Simulink. *Environ Syst Res* 4(1):24. <https://doi.org/10.1186/s40068-015-0047-9>
- Hussaian Bash C Rani C, Brisilla RM, Odofin S (2020) Mathematical design and analysis of photovoltaic cell using MATLAB/simulink. In: *Adv. Intell. Syst. Comput*. https://doi.org/10.1007/978-981-15-0035-0_58.
- Chao K-H, Ho S-H, Wang M-H (2008) Modeling and fault diagnosis of a photovoltaic system. *Electr Power Syst Res* 78(1):97–105. <https://doi.org/10.1016/j.epsr.2006.12.012>
- Salman A, Williams A, Amjad H, Bhatti MKL, Saad M (2015) Simplified modeling of a PV panel by using PSIM and its comparison with laboratory test results. In: *Proceedings of the 5th IEEE global humanitarian technology conference, GHTC 2015*. <https://doi.org/10.1109/GHTC.2015.7343997>.
- El Hammoui A, Motahhir S, Chalh A, El Ghzizal A, Derouich A (2018) Low-cost virtual instrumentation of PV panel characteristics using excel and arduino in comparison with traditional instrumentation. *Renewables Wind Water Sol*. <https://doi.org/10.1186/s40807-018-0049-0>.
- Villalva MG, Gazoli JR, Filho ER (2009) Comprehensive approach to modeling and simulation of photovoltaic arrays. *IEEE Trans Power Electron* 24(5):1198–1208. <https://doi.org/10.1109/TPEL.2009.2013862>
- Yan C, Wen Y, Jinzhao L, Jingjing B (2011,) PROTEUS-based simulation platform to study the photovoltaic cell model under partially shaded conditions. In: *2011 International conference on*

- electric information and control engineering, IEEE, pp 3446–3449. <https://doi.org/10.1109/ICEICE.2011.5778259>.
29. Chalh A, El Hammoumi A, Motahhir S, El Ghzizal A, Subramaniam U, Derouich A (2020) Trusted simulation using proteus model for a PV system: test case of an improved HC MPPT algorithm. *Energies*. <https://doi.org/10.3390/en13081943>
 30. Yaqoob SJ, Obed AA (2020) Modeling, simulation and implementation of PV system by proteus based on two-diode model. *J Tech*. <https://doi.org/10.51173/jt.v1i1.43>
 31. Yaqoob SJ, Motahhir S, Agyekum EB (2022) A new model for a photovoltaic panel using Proteus software tool under arbitrary environmental conditions. *J Clean Prod* 333:130074. <https://doi.org/10.1016/j.jclepro.2021.130074>
 32. Loukriz A, Drif M, Bouchelaghem A, Saigaa D, Bendib A, Moadh K (2022) Current balancing and PSO methods-based PV array output power optimization: a comparative study. In: 2022 International conference of advanced technology in electronic and electrical engineering (ICATEEE), IEEE, pp 1–6. <https://doi.org/10.1109/ICATEEE57445.2022.10093690>.
 33. Yang B et al (2023) Salp swarm optimization algorithm based MPPT design for PV-TEG hybrid system under partial shading conditions. *Energy Convers Manag*. <https://doi.org/10.1016/j.enconman.2023.117410>

Publisher's Note Springer Nature remains neutral with regard to jurisdictional claims in published maps and institutional affiliations.

Springer Nature or its licensor (e.g. a society or other partner) holds exclusive rights to this article under a publishing agreement with the author(s) or other rightsholder(s); author self-archiving of the accepted manuscript version of this article is solely governed by the terms of such publishing agreement and applicable law.